Supporting Information

Characterizing Slow Chemical Exchange in Nucleic Acids by Carbon CEST and Low Spin-lock Field $R_{1\rho}$ NMR Spectroscopy

Bo Zhao,[†,‡] Alexandar L. Hansen,[§] and Qi Zhang*[,†]

[†]Department of Biochemistry and Biophysics and [‡]Department of Chemistry, University of North Carolina at Chapel Hill, Chapel Hill, NC 27599, United States

[§]Departments of Molecular Genetics, Biochemistry and Chemistry, The University of Toronto, Toronto, ON M5S 1A8, Canada

Supporting Material and Methods

Sample preparation. Unlabeled and guanosine-specifically $^{13}C/^{15}N$-labeled fluoride riboswitch samples were prepared by *in vitro* transcription using T7 polymerase (P266L mutant)[1] with synthetic DNA templates as previously described.[2] The RNA construct was derived from a *Bacillus cereus* fluoride riboswitch,[3] where the P2 loop (GCUU) was replaced with a stable cUUCGg tetraloop and A9-U42 base pair was flipped to U9-A42 to minimize spectral overlap. The *in vitro* transcribed RNA samples were ethanol precipitated, gel purified (15% denaturing polyacrylamide gel), electro-eluted with the Elutrap system (Whatman), and anion-exchange purified with a 5ml Hi-Trap Q column (GE Healthcare). Using Amicon filtration with 3K MW cut-off membranes (Millipore), the RNA samples were desalted, initially exchanged to water, subsequently exchanged to 10 mM sodium phosphate (pH 6.4), 50mM KCl, and 50μM EDTA, and finally concentrated to ~1mM concentration. For fluoride-bound samples, RNAs were further exchanged to the same buffer conditions with additional 1mM $MgCl_2$ and 10mM NaF. For H_2O sample, 5% D_2O was added. For the D_2O sample, the corresponding H_2O sample was repeatedly lyophilized and re-dissolved in the same volume of 99.996% D_2O (Sigma).

NMR Spectroscopy and Data analysis. All NMR experiments were carried out on a Bruker Avance III 600 spectrometer equipped with 5mm triple-resonance cryogenic probes at either 298K or 303K. The 1D ^{1}H spectra were recorded using unlabeled H_2O samples, whereas ^{13}C CEST, $R_{1\rho}$ relaxation dispersion, and ZZ-exchange experiments were recorded using a G-labeled D_2O sample. The imino proton assignments of both free and fluoride-bound riboswitches were obtained using 2D 11echo-NOESY experiments on unlabeled H_2O samples.[4] The C8H8 assignments of ligand-free G-labeled riboswitch were obtained using ^{1}H-^{13}C HSQC and ^{13}C ZZ-exchange experiments in the presence of various magnesium and fluoride concentrations that gave cross peaks to the fully-bound riboswitch, whose assignments were obtained using standard 2D NOESY, ^{1}H-^{13}C HSQC, ^{1}H-^{15}N HSQC, HCCNH TOCSY, and HCN experiments on unlabeled and G-labeled H_2O and D_2O samples.[4-6] The C1'H1' assignments of ligand-free G-labeled riboswitch were obtained using HCN experiments[5] and the C8H8 assignments of ligand-free G-labeled riboswitch. All NMR spectra were processed and analyzed using NMRPipe/NMRDraw,[7] NMRView,[8] and Sparky 3.110. (University of California, San Francisco, CA).

2D ^{13}C CEST

The pulse sequence for the 2D ^{13}C CEST experiment is shown in Figure 1 of the main text, and is based on a gradient-sensitivity-enhanced HSQC scheme[9] and the 2D ^{15}N CEST experiment[10]. This experiment is similar to the one used for measuring carbon longitudinal relaxation rate (R_1),[11] except a weak carbon B_1 field (~10-50 Hz) is applied at different offsets during the relaxation period (T_{EX}). Narrow (wide) rectangles are hard 90° (180°) pulses, and close (open) shapes are selective on (off) resonance 180^{o} pulses. All pulses are applied along the *x*-axis unless indicated otherwise and all phases are for Bruker Spectrometers. Shaped pulse *a* selectively inverts carbon magnetization of interest while shaped pulse *b* and *c* selectively refocus and invert carbon magnetization to refocus carbon-carbon scalar couplings. During the T_{EX} period, with weak ^{13}C B_1 field being

applied, a $90_x240_y90_x$ composite pulse train,[12] as previously described by Kay and co-workers,[10] is used for ^{1}H decoupling to suppress C-H cross relaxation, C-H dipolar-dipolar/carbon CSA cross-correlated relaxation, and the ^{13}C multiplet structure in the CEST profile.[10] The ^{1}H carrier is kept on water resonance throughout the experiment except during the T_{EX} period, where it is shifted to the center of the region of interest. The ^{13}C carrier is also kept on-resonance throughout the experiment and is shifted to a desired offset during the T_{EX} period. Inter-pulse delays are $\tau = 1/4J_{CH}$ and $\tau' = g_8$. The phase cycle used is $\phi_1 = \{x, -x\}$, $\phi_2 = \{y\}$, $\phi_3 = \{2x, 2y, 2(-x), 2(-y)\}$, $\phi_4 = \{4x, 4(-x)\}$, $\phi_5 = \{4x, 4(-x)\}$, $\phi_6 = \{4y, 4(-y)\}$, receiver = $\{x, -x, -x, x, -x, x, x, -x\}$. A minimum of four scans can be used. Gradients with smoothed-square shape (SMSQ10.100) profile are applied with the following strength (G/cm)/duration (ms): g_1 = -33/0.8, g_2 = 4.62/0.6, g_3 = 46.2/0.8, g_4 = 46.2/0.8, g_5 = 59.4/0.6, g_6 = 4.62/0.6, g_7 = 4.62/0.6, g_8 = 29.9/0.6. Quadrature detection is achieved using an enhanced sensitivity gradient scheme in which separate data sets are recorded during t_1 period with (ϕ_6, g5) and ($\phi_6 + 180^o$, -g5), and axial peaks are shifted to the edge of the spectrum by incrementing ϕ_2 and receiver phase by 180^o for each t_1 increment. ^{13}C and ^{15}N decoupling during acquisition are achieved using 2.5 kHz GARP and 1.25 kHz WALTZ-16, respectively. To ensure uniform heating for experiments with variable lengths of T_{EX}, a heat compensation scheme is employed after the acquisition with length of T_{MAX} - T_{EX}, where T_{MAX} is the maximum relaxation delay time, and far off-resonance for both ^{1}H and ^{13}C channels. The third 90^o (-x) on the proton channel (prior to T_{EX} period) serves to eliminate any potential ^{13}C anti-phase magnetization prior to the spin lock period.[10,13-15] It is also worth noting that, although two identical gradients g4 were used in our experiments, they can be optimized separately to improve residual water suppression and avoid potential refocusing of undesired magnetization. For all 2D ^{13}C CEST experiments, spectra with various B_1 offsets and a 3.5 kHz field $90_x240_y90_x$ pulse were recorded with a recycle delay of 1.5 s, T_{EX} = 0.3 s, and T_{MAX} = 0.305 s. Three spectra with T_{EX} = 0 s were recorded for reference in data fitting and error estimation.

For the CEST experiment on base carbon C8s, the ^{13}C carrier was set to 135.6 ppm with a spectral width of 6.5 ppm. Selective pulses *a*, *b*, and *c* were 750 μs Q3 (on-resonance), 1000 μs reburp (on-resonance), 500 μs isnob2 (-5.89 kHz off-resonance), respectively. Three ^{13}C B_1 fields were used: for $\omega/2\pi$ = 17.68 Hz, the ^{13}C offset ranged between -990 to 990 Hz with a spacing of 30 Hz; for $\omega/2\pi$ = 27.90 and 48.21 Hz, the ^{13}C offset ranged between -1000 to 1000 Hz with a spacing of 40 and 50 Hz, respectively. A total of 168 2D spectra were recorded. For the CEST experiment on sugar carbon C1's, the ^{13}C carrier was set to 88.75 ppm with a spectral width of 4.2 ppm. Selective pulses *a*, *b*, and *c* were 1250 μs Q3 (0.6 kHz off-resonance), 1250 μs reburp (1 kHz off-resonance), 600 μs iburp2 (-5.76 kHz off-resonance), respectively. Three ^{13}C B_1 fields were used: for $\omega/2\pi$ = 17.68 Hz, the ^{13}C offset ranged between -720 to 720 Hz with a spacing of 30 Hz; for $\omega/2\pi$ = 27.90 and 37.84 Hz, the ^{13}C offset ranged between -720 to 720 Hz with a spacing of 40 Hz. A total of 132 2D data were recorded. The spin-lock powers were calibrated according to the 1D approach by Guenneugues et al.[16] using the 2D ^{13}C CEST pulse sequence shown in Figure 1 in the main text and focusing on isolated resonances that belong to residues with no exchange.

1D ^{13}C CEST

The pulse sequence for selective 1D ^{13}C CEST is shown in Figure S5, and is built on the selective 1D ^{13}C $R_{1\rho}$ RD pulse scheme.[17] The main difference between these two experiments is simply the removal of the two pulses to prepare the magnetization from Z to the effective magnetic field prior to the spin-lock and to return the magnetization back to Z after the spin-lock. For all 1D ^{13}C CEST experiments, spectra were recorded with a recycle delay of 1.5 s, T_{EX} = 0.3 s, and T_{MAX} = 0.305 s. Delay τ_{eq} was set to 30 and 50 ms for experiments at 30°C and 25°C, respectively. Three spectra with T_{EX} = 0 s were recorded for reference in data fitting and error estimation. For base carbon C8s of G8 and G10, three ^{13}C B_1 fields are used: for $\omega/2\pi$ = 17.68 Hz, the ^{13}C offset ranged between -

1200 to 600 Hz with a spacing of 30 Hz; for ω/2π = 27.90 and 48.21 Hz, the ^{13}C offset ranged between -1200 to 600 Hz with a spacing of 40 and 50 Hz, respectively. For C8 of G33, the ^{13}C offset ranged from -800 to 800 Hz with a spacing of 40 Hz for ω/2π = 27.90 Hz and a spacing of 50 Hz for ω/2π = 48.21 Hz. For sugar carbon C1's of G8 and G10, three ^{13}C B_1 fields are used: for ω/2π = 17.68 Hz, the ^{13}C offset ranged between -520 to 920 Hz with a spacing of 30 Hz; for ω/2π = 27.90 and 37.84 Hz, the ^{13}C offset ranged between -520 to 920 Hz with a spacing of 40 Hz. For C1' of G33, the ^{13}C offset ranged from -600 to 600 Hz with a spacing of 40 Hz for ω/2π = 27.90 and 37.84 Hz.

CEST Data Analysis

CEST profiles were obtained by normalizing the peak intensity as a function of spin-lock offset Ω, where $\Omega = \omega_{rf} - \Omega_{obs}$ is the frequency difference between the spin-lock carrier (ω_{rf}) and the observed peak (Ω_{obs}), to the peak intensity recorded at T_{EX} = 0 s. The profiles were fitted to a two-state exchange model between ground state (*G*) and excited state (*E*) based on the Bloch-McConnell equations,[18]

$$\frac{d}{dt}\begin{pmatrix} E/2 \\ I_x^G \\ I_y^G \\ I_z^G \\ I_x^E \\ I_y^E \\ I_z^E \end{pmatrix} = \begin{pmatrix} 0 & 0 & 0 & 0 & 0 & 0 & 0 \\ 0 & -R_2^G - k_{GE} & -\omega_G & \omega_1 & k_{EG} & 0 & 0 \\ 0 & \omega_G & -R_2^G - k_{GE} & 0 & 0 & k_{EG} & 0 \\ 2R_1^G p_G & -\omega_1 & 0 & -R_1^G - k_{GE} & 0 & 0 & k_{EG} \\ 0 & k_{GE} & 0 & 0 & -R_2^E - k_{EG} & -\omega_E & \omega_1 \\ 0 & 0 & k_{GE} & 0 & \omega_E & -R_2^E - k_{EG} & 0 \\ 2R_1^E p_E & 0 & 0 & k_{GE} & -\omega_1 & 0 & -R_1^E - k_{EG} \end{pmatrix} \begin{pmatrix} E/2 \\ I_x^G \\ I_y^G \\ I_z^G \\ I_x^E \\ I_y^E \\ I_z^E \end{pmatrix}$$

where $R_1^{G/E}$ is the longitudinal relaxation rate of the ground/excited state, $R_2^{G/E}$ is the transverse relaxation rate of the ground/excited state, ω_G and ω_E are the offsets of the applied ^{13}C B_1 field (strength of ω_1) from states G and E (ω_G is obtained from the observed ground-state peak position and $\omega_E = \omega_G + \Delta\omega$, where Δω is the chemical shift difference between the ground and excited state). The population of ground and excited states are p_G and p_E, and the rate constants are defined as $k_{GE} = p_E k_{ex}$ and $k_{EG} = p_G k_{ex}$,

where $k_{ex} = k_{GE} + k_{EG}$ is the rate of exchange. Magnetizations at the beginning of the T_{EX} period are along Z and are assumed to be in equilibrium between ground and excited states, either due to non-selective excitation in the 2D experiment (neglecting relaxation differences during INEPT transfer) or due to long equilibration time (τ_{eq}) after selective excitation of ground state in the selective 1D experiment to allow equilibration between ground and excited states magnetizations. Therefore the initial magnetization condition at $T_{EX} = 0$ is set to $I_z^G = p_G$, $I_z^E = p_E$, $I_{x,y}^{G/E} = 0$. To account for phase cycling in the pulse sequence, an additional set of initial magnetization condition is set to $I_z^G = -p_G$, $I_z^E = -p_E$, $I_{x,y}^{G/E} = 0$. The difference in I_z^G between the two initial conditions is calculated after a period of T_{EX} for the CEST profile fitting.[10] The profiles were fit using an in-house MATLAB® program with a Levenberg-Marquardt algorithm and chi-square values $\chi^2 = \sum^{N}\left(\left(I_i^{\exp} - I_i^{calc}\right)/\sigma_i^{\exp}\right)^2$ were calculated. Fitting errors were estimated from both the Jacobian output and from 200 Monte-Carlo simulations[19], and the larger errors from these two methods were reported. For analysis of CEST profiles from individual spins, the fitting parameters are $R_1 = R_1^G = R_1^E$, R_2^G, R_2^E, $\Delta\omega$, k_{ex}, and p_E. Here, we assumed that $R_1^G = R_1^E$, as the data does not constrain determination of R_1^E, however, varying R_1^E ± 2 s^{-1} from R_1^G were shown to minimally effect the exchange parameters and chi-squared values. On the other hand, R_2^G and R_2^E were used during the analysis, as assuming $R_2^G = R_2^E$ gave substantial offsets in the fitted exchange parameters as well as much lager chi-squareds. For C1' CEST profiles, an average C-C scalar coupling of 45 Hz due to C2', which was measured from a non-decoupled HSQC experiment, were implemented to calculate two CEST profiles, one representative of C2' in the 'down' state and another in the 'up' state.[20] The two CEST profiles were then averaged in the resulting fit to obtain the observed CEST profile. For global fitting, spin-specific R_1, R_2^G, R_2^E, and $\Delta\omega$ were used, while k_{ex}, and p_E are input as global exchange parameters.

1D ^{13}C Relaxation Dispersion

The on- and off-resonance relaxation dispersion profiles were measured using the recently developed 1D selective $R_{1\rho}$ experiment by Al-Hashimi and co-workers.[17] A constant-time approach described by Kay and co-workers[21] was also adapted, where $R_{1\rho}$ values were obtained from a single delay period (T_{EX} = 32 ms) and only the magnetization associated with the ground state was prepared and rotated into the effective magnetic field prior to the spin-lock. With this approach, minor modifications have been made in the pulse sequence,[17] where τ_{eq} was set to zero and the purge pulse element for suppressing water was not included. Proton decoupling during the relaxation period was achieved using CW with 8 kHz field strength. For base carbon C8s of G8 and G10, three ^{13}C spin-lock fields were used: $\omega/2\pi$ = 48.21, 102.4, and 152.5 Hz with the ^{13}C offset ranging between -1200 to 600 Hz and a spacing of 50 Hz. For sugar carbon C1's of G8 and G10, three ^{13}C spin-lock fields were used: $\omega/2\pi$ = 152.5, 201.9, and 252.0 Hz with the ^{13}C offset ranging between -550 to 950 Hz and a spacing of 50 Hz. For C8 and C1' of residue G33, the ^{13}C offset was set to from -800 to 800 Hz with spacing of 100 Hz, with a smaller spacing of 50 Hz when the ^{13}C offset ranged from -200 to 200 Hz. The spin-lock power of 48.21 Hz was adapted from the CEST experiment, and the remaining spin-lock powers were calibrated as described previously.[17] Relaxation rates were calculated as $R_{1\rho} = -\ln(I_t / I_0) / T_{EX}$, where T_{EX} = 32 ms, I_t is the decay intensity, and I_0 is the reference intensity. Relaxation rates errors were estimated by intensity deviations among three duplicates at T_{EX} = 0 ms and the signal-to-noise ratios in 1D spectra. The larger of the two errors was reported.

Relaxation Dispersion Data Analysis

Dispersion profiles were obtained by measuring the rate of decay of magnetization over the spin-lock period as a function of spin-lock offset Ω, where $\Omega = \omega_{rf} - \Omega_{obs}$ is the frequency difference between the spin-lock carrier (ω_{rf}) and the observed peak (Ω_{obs}).

Please note, this definition of offset Ω, which is different from the commonly used Ω = Ω_{obs} - ω_{rf}, is used to be consistent with the CEST profiles. The $R_{1\rho}$ values of the ground state are calculated based on to a two-state exchange model between ground state (*G*) and excited state (*E*) using on the Bloch-McConnell equation,[18]

$$\frac{d}{dt}\begin{pmatrix} I_x^G \\ I_y^G \\ I_z^G \\ I_x^E \\ I_y^E \\ I_z^E \end{pmatrix} = \begin{pmatrix} -R_2^G - k_{GE} & -\omega_G & 0 & k_{EG} & 0 & 0 \\ \omega_G & -R_2^G - k_{GE} & -\omega_1 & 0 & k_{EG} & 0 \\ 0 & \omega_1 & -R_1^G - k_{GE} & 0 & 0 & k_{EG} \\ k_{GE} & 0 & 0 & -R_2^E - k_{EG} & -\omega_E & 0 \\ 0 & k_{GE} & 0 & \omega_E & -R_2^E - k_{EG} & -\omega_1 \\ 0 & 0 & k_{GE} & 0 & \omega_1 & -R_1^E - k_{EG} \end{pmatrix} \begin{pmatrix} I_x^G \\ I_y^G \\ I_z^G \\ I_x^E \\ I_y^E \\ I_z^E \end{pmatrix}$$

The definition of all the parameters are the same as described above for CEST data analysis. Because only ground-state magnetization is present prior to the spin-lock and is prepared into the effective magnetic field for relaxation, the initial magnetization at T_{EX} = 0 is set to $I_x^G = p_G \sin(\theta)$, $I_y^G = 0$, $I_z^G = p_G \cos(\theta)$, and $I_{x,y,z}^E = 0$, where $\theta = \arctan(\omega_1 / \Omega)$ is the effective tilt angle. After the exchange period, the total magnetization is retuned back to Z with a unit vector (sinθ 0 cosθ 0 0 0) as previously described,[21] and the ground state Z magnetization (I_Z^G) is used to calculate the value $R_{1\rho} = -\ln(I_{z,t}^G / I_{z,0}^G) / T_{EX}$. The profiles were fit using in-house MATLAB® program with a Levenberg-Marquardt algorithm and chi-squared values $\chi^2 = \sum^N \left(\left(R_{1\rho,i}^{\exp} - R_{1\rho,i}^{calc} \right) / \sigma_i^{\exp} \right)^2$ were calculated. Fitting errors were estimated from both the Jacobian output and from 200 Monte-Carlo simulations[19], and the larger errors from these two methods were reported. Because of the elevated baseline, accurate R_1^G values could not be obtained through fitting and were fixed in the fitting using the values determined by R_1 experiments. Fitting parameters are R_2^G, R_2^E, Δω, k_{ex}, and p_E. Here, we assumed that R_1^G = R_1^E, however, varying R_1^E ±2 s^{-1} from R_1^G were shown to minimally effect the exchange parameters and chi-squares. On the other hand, R_2^G and R_2^E were used during

the analysis, as assuming $R_2^G = R_2^E$ gave offsets in the fitted exchange parameters as well as lager chi-squareds. Since the spin-lock power is larger enough to decouple the C-C coupling, the C1' RD profiles were analyzed the same as C8 profiles. For global fitting, spin-specific R_2^G, R_2^E, and $\Delta\omega$ were used, whereas k_{ex}, and p_E are global exchange parameters.

^{13}C Spin Relaxation

Longitudinal (R_1) relaxation rates were measured for base and sugar carbons (C8 and C1') using the 2D CEST experiment without the carbon B_1 field during the relaxation period. Relaxation delays were 0, 150, 300ms, and R_1 rates and errors for each spin of interest were determined by fitting intensities to a single-exponential decay, $I_t = I_0 e^{-R_1 t}$.

^{13}C ZZ-Exchange

The pulse sequence for 2D ^{13}C ZZ-exchange experiment is shown in Figure S4, where ^{1}H selective pulse is 2500 μs iburp2 centered on 7.65 ppm and ^{13}C selective pulses *a* and *b* are 750 μs Q3 (on-resonance) and 500 μs isnob2 (-5.5 kHz off-resonance), respectively. The ^{13}C carrier was set to 135.6 ppm with a spectral width of 7.5 ppm. The mixing times were 5 (x2), 10, 15, 25, 50 (x2), 75, 100, 200 (x2), and 500 ms for experiments at 30°C and 5 (x2), 10, 15, 25, 50 (x2), 100, 200 (x2), and 500 ms for experiments at 25°C, where duplicated measurements were indicated as x2. The intensity errors were estimated based on the signal-to-noise ratios and the deviations among duplicated measurements, which were set to be 2% for GS diagonal peaks and ES→GS cross peaks at 30°C and 3% for all the other peaks at 30°C and 25°C. The spectra with highest cross-peak intensities, including 50, 75, and 100ms mixing-time spectra at 30°C and 25, 50, and 100ms mixing-time spectra at 25°C, were used to calculate $\Delta\varpi_{GE}$.

Magnetizations for diagonal (I_{GG} and I_{EE}) and cross (I_{GE} and I_{EG}) peaks that undergo a two-state exchange model between ground state (*G*) and excited state (*E*) with different

relaxation properties of the exchanging states can be described by,[23]

$$
\begin{aligned}
I_{GG}(T) = \quad & A_G I_G(0)\left(-\left(\lambda_2 - a_{11}\right)e^{-\lambda_1 T} + \left(\lambda_1 - a_{11}\right)e^{-\lambda_2 T}\right)/\left(\lambda_1 - \lambda_2\right) \\
I_{EE}(T) = \quad & A_E I_E(0)\left(-\left(\lambda_2 - a_{22}\right)e^{-\lambda_1 T} + \left(\lambda_1 - a_{22}\right)e^{-\lambda_2 T}\right)/\left(\lambda_1 - \lambda_2\right) \\
I_{GE}(T) = \quad & A_E I_G(0)\left(a_{21}e^{-\lambda_1 T} - a_{21}e^{-\lambda_2 T}\right)/\left(\lambda_1 - \lambda_2\right) \\
I_{EG}(T) = \quad & A_G I_E(0)\left(a_{12}e^{-\lambda_1 T} - a_{12}e^{-\lambda_2 T}\right)/\left(\lambda_1 - \lambda_2\right)
\end{aligned}
$$

where $\lambda_{1,2} = \left(\left(a_{11} + a_{22}\right) \pm \sqrt{(a_{11} - a_{22})^2 + 4k_{GE}k_{EG}}\right)/2$, $a_{11} = R_1^G + k_{GE}$, $a_{12} = -k_{EG}$, $a_{21} = -k_{GE}$, $a_{22} = R_1^E + k_{EG}$, and $I_{G/E}(0)$ represents the magnetization of the ground/excited state peak at $T_{EX} = 0$. Compared with the original equation describing magnetizations during ZZ-exchange by Farrow et al.,[22] the above equation by Tollinger et al. contains two additional factors, A_G and A_E, to account for differential relaxations of magnetizations associated with the ground and excited states during the reverse INEPT step.[23] It was also noted that differential relaxations of GS and ES magnetizations during the INEPT transfer prior to the mixing period do not need to be accounted for as they are fitted in the terms $I_{G/E}(0)$.[23] Here, $A_{G,E}$ are given by $A_{G,E} = \exp\left[-\left(\overline{R}_{2,C}^{G,E} + \overline{R}_{2,H}^{G,E}\right) \times 2\tau\right]$, where $\overline{R}_{2,C}^{G,E}$ and $\overline{R}_{2,H}^{G,E}$ are average transverse relaxation rates for ^{13}C and ^{1}H magnetizations associated with ground and excited states, and $\tau = 1/4J_{CH}$ is the inter-pulse delay in Figure S4.[23] Both A_G and A_E can be calculated and input as fixed parameters once $\overline{R}_2^{G,E}$ are measured. However, since we cannot measure $\overline{R}_2^E$ s due to non-detectable ES peaks, we allowed A_E to be fitted during our analysis while keeping A_G fixed at 1 (A_G and A_E are correlated, therefore, only one parameter is fitted). It is worth noting that, while the inclusion of A_E can take the differential relaxation into account, as shown in the simulated data (Fig. S5), larger deviations in the extracted exchange parameters can be expected when A_E is fitted as a parameter. Peak volumes, which were integrated using Sparky 3.110, were fitted to the above equation using MATLAB® with a Levenberg-Marquardt algorithm and chi-squared values $\chi^2 = \sum^N \left(\left(I_i^{\exp} - I_i^{calc}\right)/\sigma_i^{\exp}\right)^2$ were calculated. Fitting errors were estimated from both the Jacobian output and from 200 Monte-Carlo simulations[19], and

the larger errors from these two methods were reported. Because the excited states cannot be observed, the data do not constrain the R_1^E values and a single R_1 was used in the data analysis. Fitting parameters are $I_G(0)$, $I_E(0)$, A_E, R_1, k_{GE}, and k_{EG}. Excited state population is calculated as $p_E = k_{GE} / k_{ex}$, where $k_{ex} = k_{GE} + k_{GE}$. For global fitting, residue-specific $I_G(0)$, $I_E(0)$, A_E, and R_1 were used, and k_{GE} and k_{EG} are global exchange parameters.

Supporting Information References

(1) Guillerez, J.; Lopez, P. J.; Proux, F.; Launay, H.; Dreyfus, M. *Proc. Natl. Acad. Sci. U.S.A.* **2005**, *102*, 5958.
(2) Zhang, Q.; Kim, N. K.; Peterson, R. D.; Wang, Z.; Feigon, J. *Proc. Natl. Acad. Sci. U.S.A.* **2010**, *107*, 18761.
(3) Baker, J. L.; Sudarsan, N.; Weinberg, Z.; Roth, A.; Stockbridge, R. B.; Breaker, R. R. *Science* **2012**, *335*, 233.
(4) Dieckmann, T.; Feigon, J. *J. Biomol. NMR* **1997**, *9*, 259.
(5) Sklenar, V.; Peterson, R. D.; Rejante, M. R.; Feigon, J. *J. Biomol. NMR* **1993**, *3*, 721.
(6) Sklenar, V.; Dieckmann, T.; Butcher, S. E.; Feigon, J. *J. Biomol. NMR* **1996**, *7*, 83.
(7) Delaglio, F.; Grzesiek, S.; Vuister, G. W.; Zhu, G.; Pfeifer, J.; Bax, A. *J. Biomol. NMR* **1995**, *6*, 277.
(8) Johnson, B. A.; Blevins, R. A. *J. Biomol. NMR* **1994**, *4*, 603.
(9) Kay, L. E.; Keifer, P.; Saarinen, T. *J. Am. Chem. Soc.* **1992**, *114*, 10663.
(10) Vallurupalli, P.; Bouvignies, G.; Kay, L. E. *J. Am. Chem. Soc.* **2012**, *134*, 8148.
(11) Hansen, A. L.; Al-Hashimi, H. M. *J. Am. Chem. Soc.* **2007**, *129*, 16072.
(12) Levitt, M. H. *J. Magn. Reson.* **1982**, *50*, 95.
(13) Iwahara, J.; Jung, Y. S.; Clore, G. M. *J. Am. Chem. Soc.* **2007**, *129*, 2971.
(14) Fawzi, N. L.; Ying, J.; Ghirlando, R.; Torchia, D. A.; Clore, G. M. *Nature* **2011**, *480*, 268.
(15) Lakomek, N. A.; Ying, J.; Bax, A. *J. Biomol. NMR* **2012**, *53*, 209.
(16) Guenneugues, M.; Berthault, P.; Desvaux, H. *J. Magn. Reson.* **1999**, *136*, 118.
(17) Hansen, A. L.; Nikolova, E. N.; Casiano-Negroni, A.; Al-Hashimi, H. M. *J. Am. Chem. Soc.* **2009**, *131*, 3818.
(18) Mcconnell, H. M. *J. Chem. Phys.* **1958**, *28*, 430.
(19) Dethoff, E. A.; Petzold, K.; Chugh, J.; Casiano-Negroni, A.; Al-Hashimi, H. M. *Nature* **2012**, *491*, 724.
(20) Vallurupalli, P.; Kay, L. E. *Angew. Chem. Int. Ed. Engl.* **2013**, *52*, 4156.
(21) Korzhnev, D. M.; Orekhov, V. Y.; Kay, L. E. *J. Am. Chem. Soc.* **2005**, *127*, 713.
(22) Farrow, N. A.; Zhang, O.; Forman-Kay, J. D.; Kay, L. E. *J. Biomol. NMR* **1994**, *4*, 727.
(23) Tollinger, M.; Skrynnikov, N. R.; Mulder, F. A.; Forman-Kay, J. D.; Kay, L. E. *J. Am. Chem. Soc.* **2001**, *123*, 11341.
(24) Pelupessy, P.; Chiarparin, E.; Bodenhausen, G. *J. Magn. Reson.* **1999**, *138*, 178.

Table S1: Summary of parameters obtained from fitting CEST, *R*1ρ and ZZ-exchange data recorded at 30°C

Method	Parameter	G8/C8	G8/C1'	G10/C8	G10/C1'	G8/C8	G8/C1'	G10/C8	G10/C1'
		Global Fit				Individual Fit			
CEST	R_1 (s^{-1})	2.36 ± 0.01	2.15 ± 0.01	2.47 ± 0.01	2.25 ± 0.01	2.36 ± 0.01	2.15 ± 0.01	2.47 ± 0.01	2.24 ± 0.01
	R_{2G} (s^{-1})	23.6 ± 0.5	17.3 ± 0.5	20.0 ± 0.5	17.4 ± 0.5	24.1 ± 0.8	16.6 ± 0.7	20.8 ± 0.7	16.8 ± 0.7
	R_{2E} (s^{-1})	137 ± 6	101 ± 6	165 ± 6	171 ± 8	147 ± 7	95.4 ± 6.9	171 ± 7	162 ± 8
	$\Delta\varpi_{GE}$ (ppm)	-4.10 ± 0.01	3.40 ± 0.01	-3.96 ± 0.01	2.40 ± 0.01	-4.09 ± 0.01	3.41 ± 0.01	-3.95 ± 0.01	2.40 ± 0.01
	k_{ex} (s^{-1})	112 ± 4				109 ± 8	122 ± 7	102 ± 7	117 ± 7
	p_{ES} (%)	10.1 ± 0.1				9.86 ± 0.29	9.83 ± 0.26	10.4 ± 0.3	10.4 ± 0. 3
	χ^2 *(Reduced)*	3.62 (10.6*)				6.36 (15.5*)	1.59 (3.31*)	3.16 (11.9*)	2.36 (8.95*)
*R*1ρ	R_1 (s^{-1}) *(Input)*	2.43 ± 0.03	2.17 ± 0.07	2.48 ± 0.04	2.31 ± 0.06	2.43 ± 0.03	2.17 ± 0.07	2.48 ± 0.04	2.31 ± 0.06
	R_{2G} (s^{-1})	28.3 ± 0.2	21.0 ± 0.1	23.7 ± 0.2	21.1 ± 0.1	28.8 ± 0.2	19.9 ± 0.1	24.7 ± 0.2	20.6 ± 0.1
	R_{2E} (s^{-1})	100 ± 12	86.9 ± 11.0	97.2 ± 12.4	124 ± 12	122 ± 15	76.8 ± 10.6	131 ± 17	115 ± 13
	$\Delta\varpi_{GE}$ (ppm)	-3.96 ± 0.02	3.34 ± 0.04	-4.03 ± 0.02	2.41 ± 0.04	-3.95 ± 0.02	3.30 ± 0.03	-4.00 ± 0.02	2.38 ± 0.04
	k_{ex} (s^{-1})	121 ± 2				116 ± 2	120 ± 3	110 ± 2	116 ± 3
	p_{ES} (%)	10.8 ± 0.1				10.8 ± 0.2	11.8 ± 0.3	11.0 ± 0.2	11.7 ± 0.3
	χ^2 *(Reduced)*	6.48 (9.95*)				5.06 (8.92*)	2.53 (4.38*)	6.41 (10.9*)	3.02 (7.25*)
ZZ-exchange	R_1 (s^{-1})	2.35 ± 0.12		2.46 ± 0.13		2.35 ± 0.13		2.46 ± 0.15	
	$\Delta\varpi_{GE}$ (ppm)	4.11 ± 0.01		4.03 ± 0.01		4.11 ± 0.01		4.03 ± 0.01	
	k_{ex} (s^{-1})	78.1 ± 13.2				65.4 ± 16.5		90.0 ± 23.6	
	p_{ES} (%)	17.3 ± 5.3				16.2 ± 7.4		18.5 ± 9.4	
	χ^2 *(Reduced)*	0.40				0.40		0.40	

** Shown in parenthesis are reduced χ^2 values obtained from data fitting with $R_{2G}=R_{2E}$.*

Table S2: Summary of parameters obtained from fitting CEST, $R1\rho$ and ZZ-exchange data recorded at 25°C

Method	Parameter	G8/C8	G10/C8	G8/C8	G10/C8
		Global Fit		Individual Fit	
CEST	R_1 (s^{-1})	2.35 ±0.01	2.51 ± 0.01	2.35 ± 0.01	2.51 ± 0.01
	R_{2G} (s^{-1})	25.6 ± 0.7	20.8 ± 0.7	25.7 ± 0.8	20.4 ± 0.9
	R_{2E} (s^{-1})	154 ± 6	184 ± 7	160 ± 6	179 ± 8
	$\Delta\varpi_{GE}$ (ppm)	-4.12 ± 0.01	-4.01 ± 0.01	-4.12 ± 0.01	-4.01 ± 0.01
	k_{ex} (s^{-1})	55.1 ± 3.3		54.5 ± 4.3	57.1 ± 5.0
	p_{ES} (%)	16.5 ± 0.5		16.2 ± 0.7	16.6 ± 0.8
	χ^2 *(Reduced)*	4.37 (40.2*)		4.55 (44.1*)	4.21 (34.6*)
$R1\rho$	R_1 (s^{-1}) *(Input)*	2.33 ± 0.15	2.52 ± 0.13	2.33 ± 0.15	2.52 ± 0.13
	R_{2G} (s^{-1})	34.2 ± 0.1	27.7 ± 0.1	34.3 ± 0.2	27.6 ± 0.2
	R_{2E} (s^{-1})	116 ± 14	123 ± 15	124 ± 16	115 ± 18
	$\Delta\varpi_{GE}$ (ppm)	-3.99 ± 0.02	-4.15 ± 0.02	-3.98 ± 0.02	-4.15 ± 0.02
	k_{ex} (s^{-1})	61.3 ± 0.8		61.8 ± 1.1	60.8 ± 1.2
	p_{ES} (%)	19.9 ± 0.2		19.7 ± 0.3	20.1 ± 0.3
	χ^2 *(Reduced)*	2.15 (3.28*)		2.62 (4.03*)	1.73 (2.55*)
ZZ-exchange	R_1 (s^{-1})	2.14 ± 0.21	2.27 ± 0.21	2.12 ± 0.21	2.29 ± 0.25
	$\Delta\varpi_{GE}$ (ppm)	4.14 ± 0.01	4.08 ± 0.00	4.14 ± 0.01	4.08 ± 0.00
	k_{ex} (s^{-1})	44.0 ± 6.7		40.7 ± 7.9	47.8 ± 9.9
	p_{ES} (%)	29.5 ± 7.2		29.7 ± 8.8	29.3 ± 9.5
	χ^2 *(Reduced)*	0.30		0.40	0.30

** Shown in parenthesis are reduced χ^2 values obtained from data fitting with $R_{2G}=R_{2E}$.*

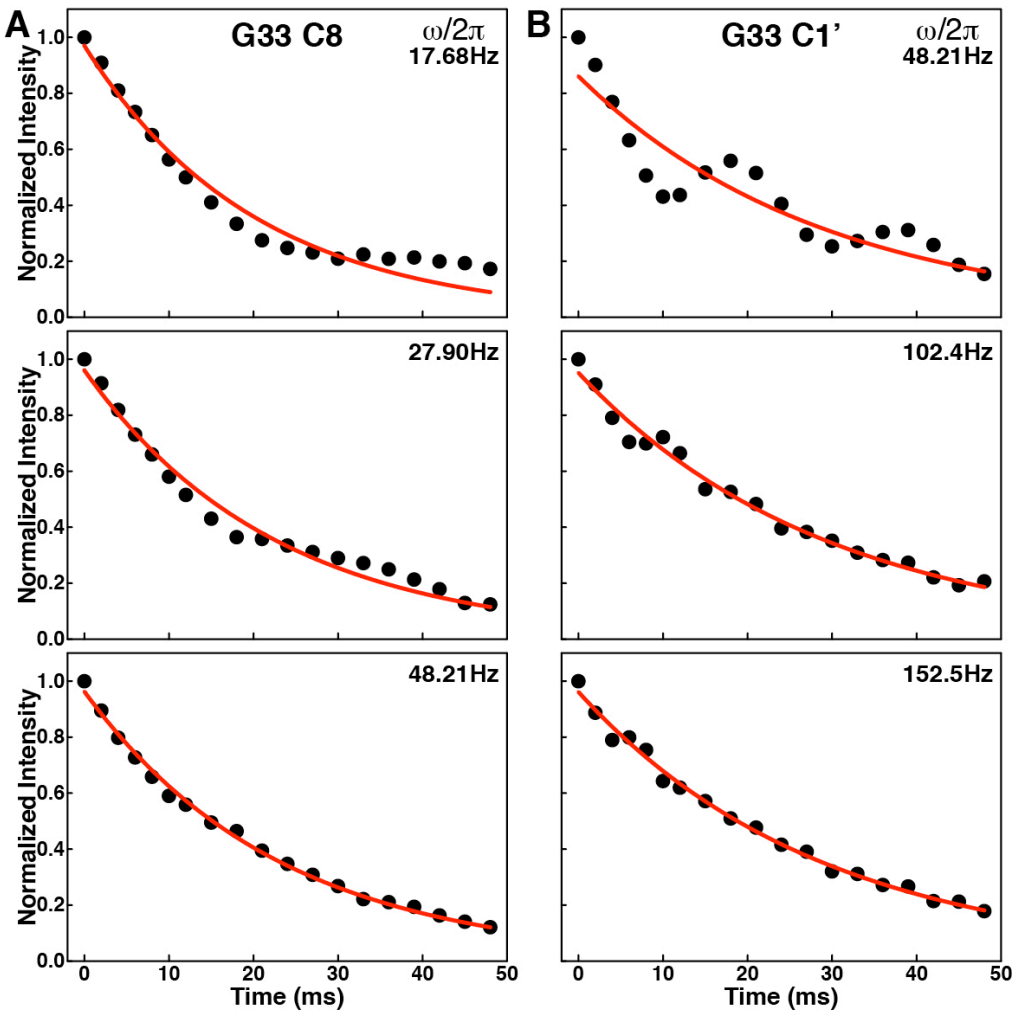

Figure S1. Assessment of low spin-lock field limit for $R_{1\rho}$ measurement. Shown are spin-lock power ($\omega/2\pi$) and time dependence of on-resonance $R_{1\rho}$ for (A) base carbon C8 and (B) sugar carbon C1' of G33, a residue with no exchange. Solid-lines represent best fit to a single exponential decay for each profile.

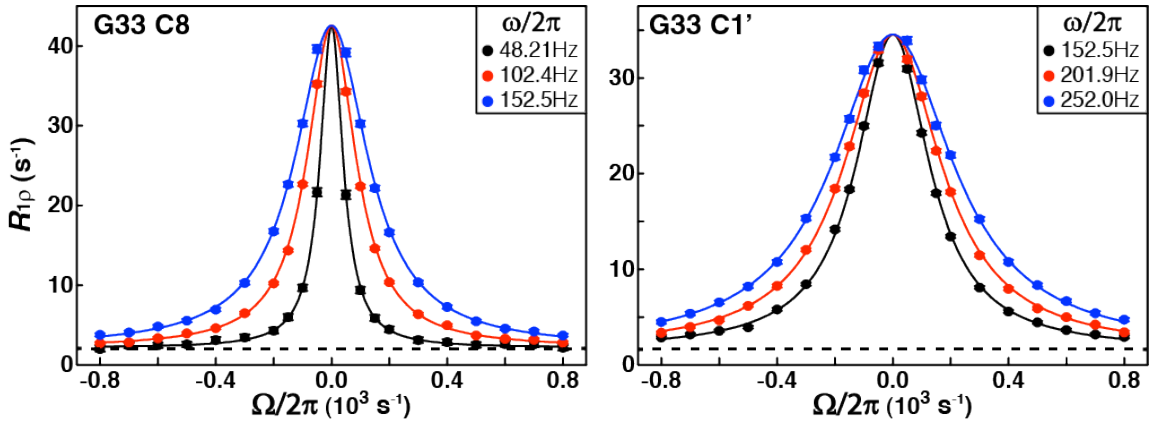

Figure S2. Relaxation dispersion profiles of G33. Shown are spin-lock power (ω/2 π) and offset (Ω/2π) dependence of $R_{1\rho}$ for base carbon C8 and sugar carbon C1', where $\Omega = \omega_{rf} - \Omega_{obs}$ is the frequency difference between the spin-lock carrier (ω_{rf}) and the observed peak (Ω_{obs}). Dashed lines are measured intrinsic R_1 rates. Solid lines represent the best fits of the dispersion profiles to $R_{1\rho} = R_1 \cos^2\theta + R_{2,0} \sin^2\theta$, where $\theta = \arctan(\omega / \Omega)$ is the effective tilt angle in the spin-lock field.

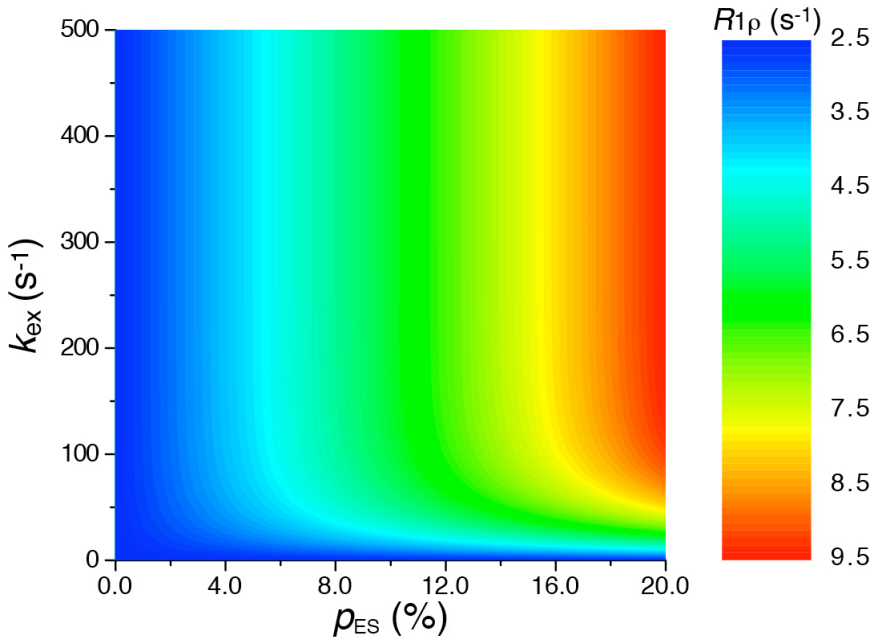

Figure S3. Examination of elevated $R_{1\rho}$ baselines in the presence of chemical exchange. Shown are simulated $R_{1\rho}$ values as functions of exchange rates (k_{ex}) and excited-state population (p_{ES}) using the Bloch-McConnell equation[18] with a condition of only ground-state magnetization existing prior to exchange[21]. To evaluate baseline elevation, $R_{1\rho}$ values were calculated using a constant mixing time of 32 ms at an offset of $\Omega/2\pi$ = 5000 Hz, a spin-lock power of $\omega/2\pi$ = 45 Hz, and other parameters being $R_{1(GS)} = R_{1(ES)} = 2.5$ s^{-1}, $R_{2(GS)} = R_{2(ES)} = 30$ s^{-1} and $\Delta\varpi$ = -3791 s^{-1} that corresponds to -4.0 ppm at 150.829 MHz.

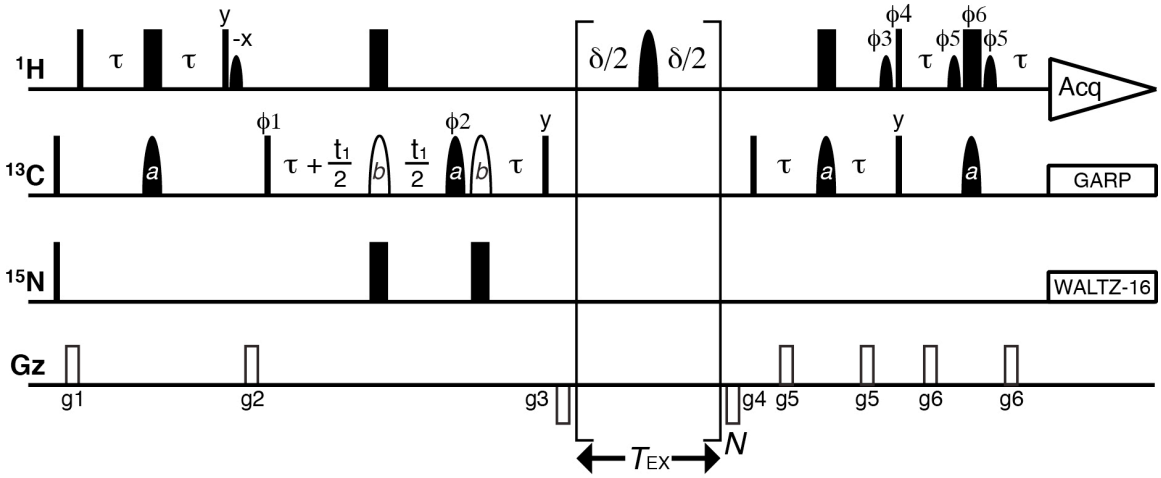

Figure S4. 2D ^{13}C ZZ-exchange pulse sequence for characterizing slow chemical exchange in nucleic acids. The sequence is based on a previously published 2D ^{15}N ZZ-exchange pulse scheme.[22] Narrow (wide) rectangles are hard 90° (180°) pulses, and close (open) shapes are selective on (off) resonance 180^o pulses, except the small shaped pulses on ^{1}H are selective 90^o pulse on water. All pulses are applied along *x*-axis unless indicated otherwise, and all phases are for Bruker Spectrometers. The ^{1}H carrier is kept on water resonance throughout the experiment, except during the T_{EX} period, it is shifted to the center of the proton region of interest. Inter-pulse delay $\tau = 1/4J_{CH}$, and delays between selective 180^o pulse during T_{EX} is δ = 5ms. Total relaxation period $T_{EX} = \delta$ *N. The phase cycle used is $\phi_1 = \{x\}$, $\phi_2 = \{4x, 4y, 4(-x), 4(-y)\}$, $\phi_3 = \{2x, 2(-x)\}$, $\phi_4 = \{2x, 2(-x)\}$, $\phi_5 = \{x, -x\}$, $\phi_6 = \{-x, x\}$, receiver = $\{x, x, -x, -x, -x, -x, x, x\}$. Gradients with SMSQ10.100 profile are applied with the following strength (G/cm)/duration (ms): g_1 = 9.9/1.0, g_2 = 23.1/1.0, g_3 = -39.6/1.0, g_4 = -19.8/1.0, g_5 = 16.5/0.5, g_6 = 16.5/0.125. Quadrature detection is achieved by incrementing ϕ_1 and receiver phase by 180^o for each t_1 increment via States-TPPI. ^{13}C and ^{15}N decoupling during acquisition are achieved using 2.5 kHz GARP and 1.25 kHz WALTZ-16, respectively.

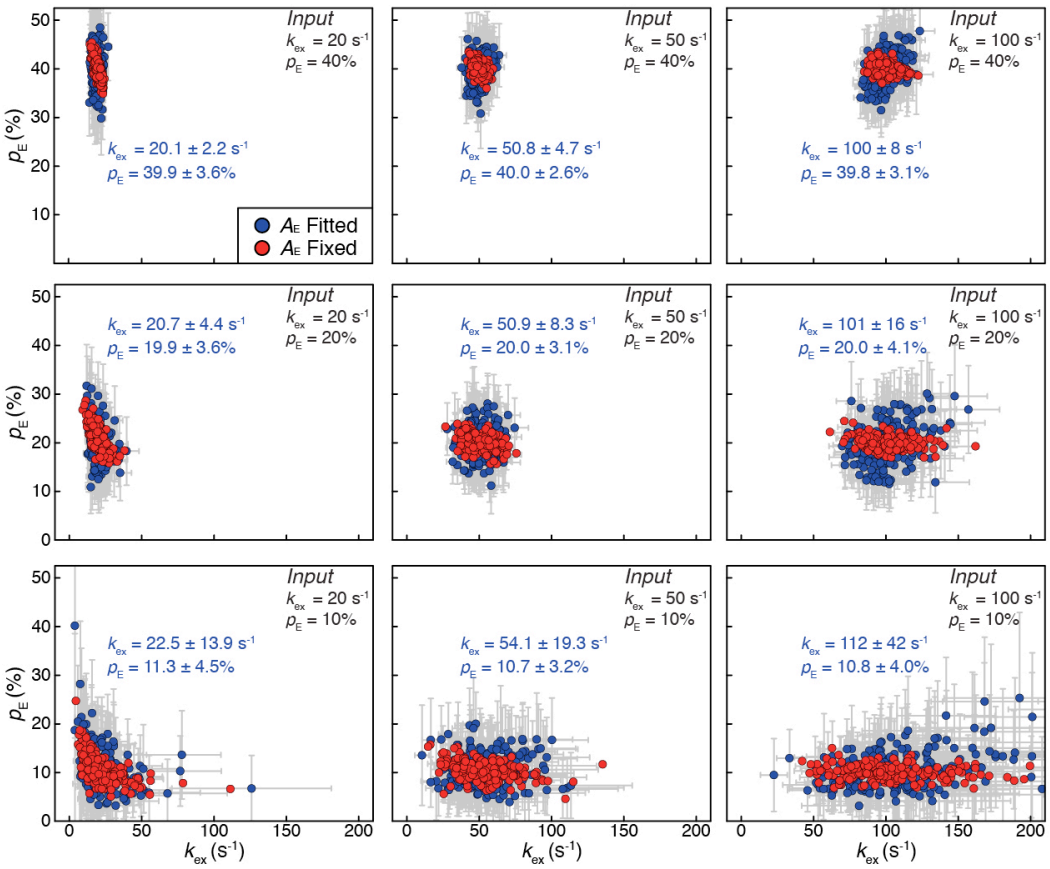

Figure S5. Examination of the utility of ZZ-exchange experiment in characterizing slow chemical exchange. To evaluate the utility of ZZ-exchange experiment that closely mimics the experimental setup where ES diagonal-peak cannot be observed, synthetic intensities for GS diagonal-peak and cross-peaks between GS and ES were calculated using the ZZ-exchange equations at T_{EX} = 5, 10, 15, 25, 50, 75, 100, 200, and 500 ms with k_{ex} = 20, 50, 100 s^{-1}, p_E = 10, 20, 40%, R_1 = 2.5 Hz, A_G = 1, and A_E = 0.6 (assuming ΔR_2s ~ 100 s^{-1} between GS and ES). A Gaussian error corresponding to the lowest experimental error (2% of p_G) was then randomly added to each synthetic intensity to generate a total of 200 randomly perturbed data sets. These 200 data sets were fitted individually to the ZZ-exchange equations to extract k_{ex} and p_E values. Shown are the distributions of k_{ex} and p_E obtained from above analysis either fixing A_E at 0.6 (red) or allowing A_E to be fitted (blue), which mimics the situations where R_2 (ES) either can be experimental measured or can not due to non-detectable ES peaks. For clarity, only the error bars (one s.d.) associated with blue circles are shown. The k_{ex} and p_E values shown in the figure are mean ± standard deviation for the 200 best-fit values. It can be clearly seen that the accuracy of extracted exchange parameters from ZZ-exchange highly depends on the population of the exchanging states. When p_E is low, small measurement errors can result in large deviations in extracted exchange parameters, where the best-fit values can be more than 1 s.d. away from the true value. This is also consistent with the commonly knowledge that the application of ZZ-exchange in studying slow exchange requires exchanging states to be sufficiently populated.

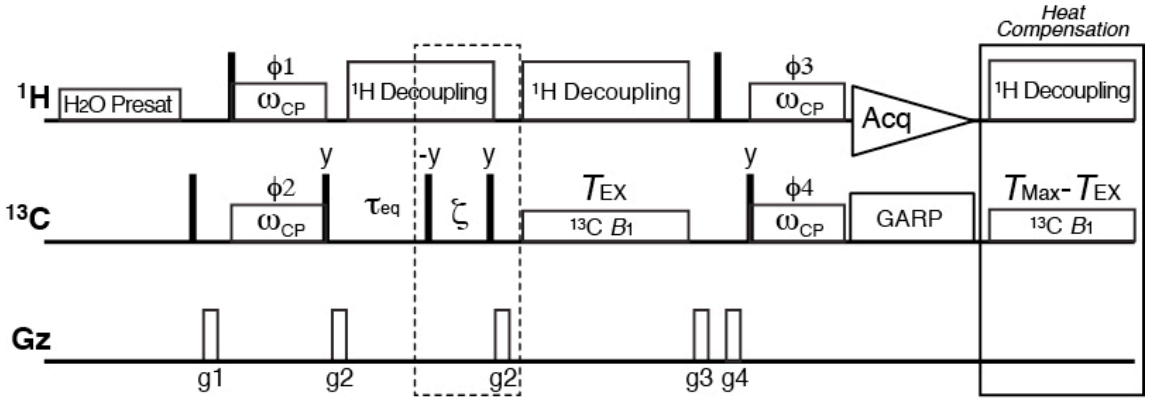

Figure S6. 1D ^{13}C CEST pulse sequence for characterizing slow chemical exchange in nucleic acids. This sequence is developed built on the 1D ^{13}C-$R_{1\rho}$ RD pulse scheme by Al-Hashimi and co-workers.[17] Narrow and open rectangles are hard 90° pulses and weak continuous-wave irradiations for water preset, cross-polarization transfer, ^{1}H decoupling, and applied ^{13}C B_1 fields, respectively. All pulses are applied along x-axis unless indicated otherwise, and all phases are for Bruker Spectrometers. During the T_{EX} period with a weak ^{13}C B_1 field being applied, a $90_x240_y90_x$ composite pulse[12] of 3.5 kHz, as previously described by Kay and co-workers,[21] is used for ^{1}H decoupling to suppress C-H cross relaxation and C-H dipolar-dipolar/carbon CSA cross-correlated relaxation. The ^{1}H carrier is on water resonance, and is shifted to the center of the proton region of interest before the first CP transfer and is returned back to water resonance before acquisition. The ^{13}C carrier is kept on-resonance throughout the experiment, and is shifted to a desired offset during the T_{EX} period. CP transfer is achieved by ~100 Hz spin-lock field for 4500 μs.[17,24] The optional ζ delay (dotted line) can be used to suppress ^{13}C signals with similar ^{1}H frequencies, as described previously.[17,21] Delay τ_{eq} (~3-5/k_{ex}) is used to equilibrate exchanging spins in the 1D CEST experiment. The phase cycle used is ϕ_1 = {8y, 8(-y)}, ϕ_2 = {-x, x}, ϕ_3 = {4x, 4(-x)}, ϕ_4 = {2x, 2(-x)}, receiver = {x, -x, -x, x, 2(-x, x, x, -x), x, -x, -x, x}. Gradients with SMSQ10.100 profile are applied with the following strength (G/cm)/duration (ms): g_1 = 28.38/0.5, g_2 = 58.74/0.5, g_3 = 47.78/0.5, g_4 = 40.26/0.5. ^{13}C and ^{15}N decoupling during acquisition are achieved using 2.5 kHz GARP and 1.25 kHz WALTZ-16, respectively. To ensure proper heating with various lengths of T_{EX}, a heat compensation scheme is employed after the acquisition with length of T_{MAX} - T_{EX}, where T_{MAX} is the maximum relaxation delay time, and is applied far off-resonance for both ^{1}H and ^{13}C channels.

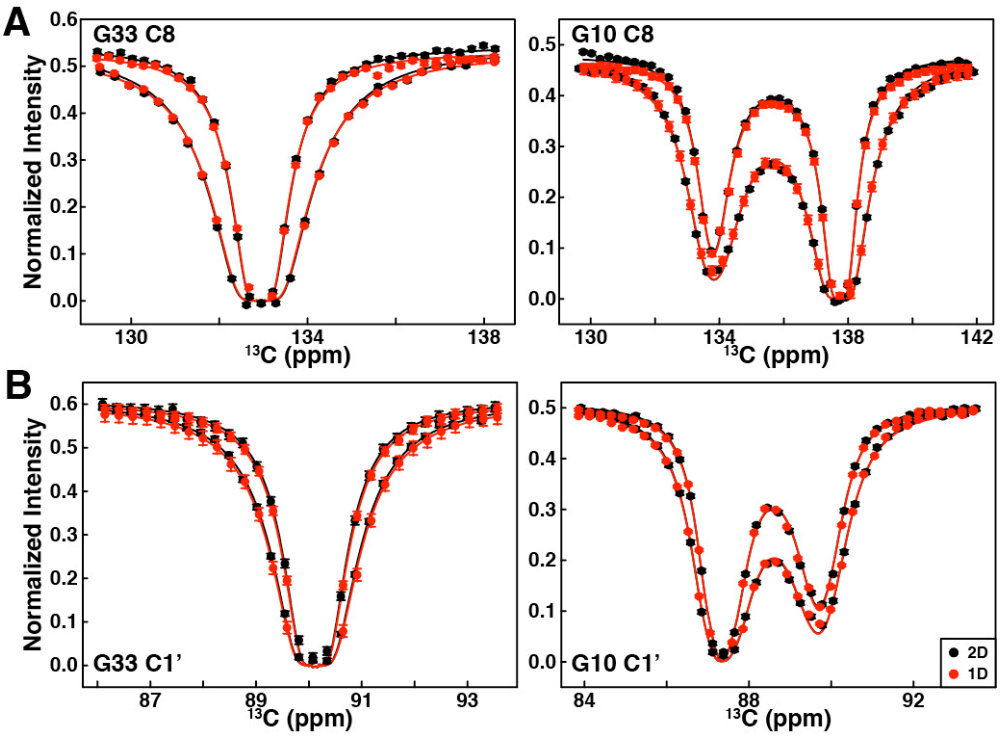

Figure S7. Comparison of 1D and 2D CEST profiles. (A-B) B_1 field strength (27.90 and 48.21 Hz) and carrier (in ppm) dependence of intensity profiles of base C8s and sugar C1's for G33 and G10 recorded using the 1D CEST (red) and 2D CEST (black) experiments. Solid lines represent the best fits for 1D (red) and 2D (black) profiles.

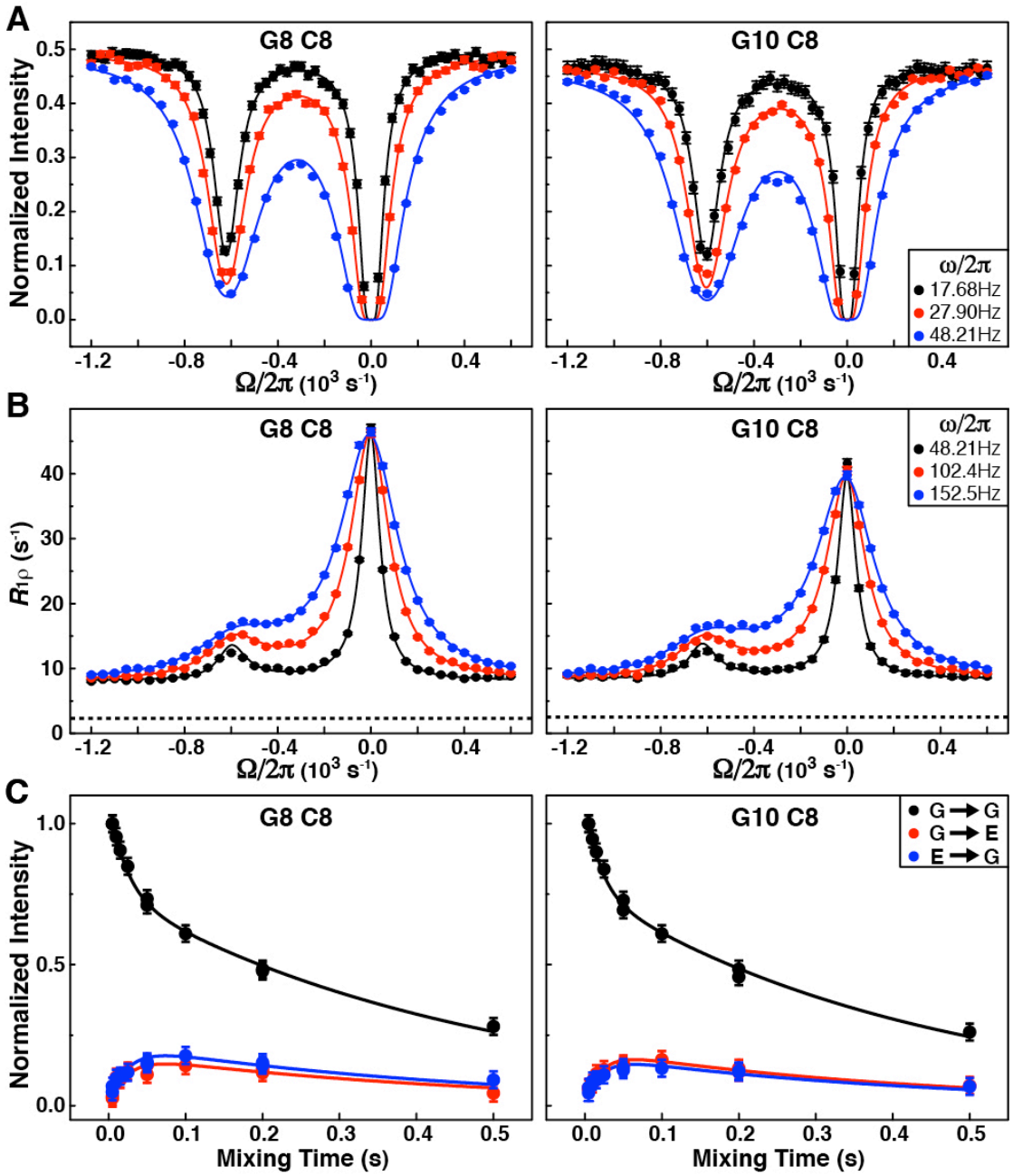

Figure S8. Quantification of slow chemical exchange in ligand-free *Bacillus cereus* fluoride riboswitch at 25°C. (A) B_1 field strength and carrier (in ppm) dependence of intensity profiles of base C8s for G8 and G10. Solid lines represent the best individual fits to a two-state exchange process using the Bloch-McConnell equation.[18] (B) Shown are spin-lock power ($\omega/2\pi$) and offset ($\Omega/2\pi$) dependence of $R_{1\rho}$ for base carbon C8s of G8 and G10, where $\Omega = \omega_{rf} - \Omega_{obs}$ is the frequency difference between the spin-lock carrier (ω_{rf}) and the observed peak (Ω_{obs}). Dashed lines are measured intrinsic R_1 rates for each spin. Solid lines represent the best individual fits to a two-state exchange process using the Bloch-McConnell equation. (C) Mixing-time dependence of intensities of auto- and cross-peaks for G8 and G10 from ZZ-exchange experiment. Solid lines represent the best individual fits to a two-state exchange process.